Electronic structure of Millerite NiS

S. R. Krishnakumar, N. Shanthi and D. D. Sarma*

Solid State and Structural Chemistry Unit, Indian Institute of Science, Bangalore, 560012, India

(February 1, 2008)

Abstract

We investigate the electronic structure of Nickel sulphide (NiS) in the millerite phase using electron spectroscopic measurements and band structure as well as model Hamiltonian calculations. While band structure calculations are found to be relatively more successful in describing the experimental valence band spectrum of this highly conducting phase compared to the hexagonal phase of NiS, cluster calculations including electron correlation effects are found to be necessary for the description of certain features in the experimental spectra, indicating importance of correlation effects even in a highly metallic system. The electronic parameter strengths obtained from these calculations confirm that the millerite NiS is a highly covalent *pd*-metal. The comparative study of hexagonal and millerite forms of NiS, provides the information concerning the evolution of the spectral function in a *pd*-metal as a function of covalency.

PACS Numbers: 71.28.+d, 79.60.Bm, 71.45.Gm, 71.30.+h

I. INTRODUCTION

There have been numerous electron spectroscopic investigations of the metastable hexagonal phase of nickel monosulphide (NiS), primarily to understand its unusual electronic phase transition [1,2]. However, no electron spectroscopic studies have been undertaken on the millerite phase of NiS, which is the *stable phase* below 600 K. The resistivity measurements on the system show that it has a high metallic conductivity ($\sim 2 \times 10^4$ Ohms^{-1}-cm^{-1} at room temperature). It has been speculated [3,4] that the millerite phase is diamagnetic with the observed small magnetic susceptibility attributed to the presence of paramagnetic hexagonal modification of NiS. Millerite NiS crystallizes in the lower symmetry trigonal space group ($R3m$) with lattice parameters $a = 9.589$ Å and $c = 3.165$ Å [5]. The crystal structure of millerite NiS is shown in Fig. 1(a). Here, the Ni atom has five nearest neighbor S atoms, occupying the corners of a square pyramid. In this pyramidal geometry (see Fig. 1(b)) the Ni atoms are displaced slightly out of the basal plane, towards the apical sulphur atom. Though the local coordination of Ni in millerite is very similar to that in another Ni-S system, $BaNiS_2$, millerite has a three-dimensional structure in contrast to $BaNiS_2$ which is highly two-dimensional in nature. The Ni-S bond in millerite NiS (shortest $d_{Ni-S} = 2.25$ Å) is relatively shorter than that in hexagonal NiS ($d_{Ni-S} = 2.39$ Å), NiS_2 ($d_{Ni-S} = 2.40$ Å) or $BaNiS_2$ (shortest $d_{Ni-S} = 2.32$ Å) and leads to stronger hybridization effects in this system.

There have been very few studies to understand the electronic structure of this compound. Band structure calculation performed for the millerite phase of NiS [6] showed the ground state to be metallic, in agreement with experimental results. However, no comparison between experimental and theoretical results exists and the details of the electronic structure in terms of the electronic structure parameters are still unknown.

In the present study, we investigate the electronic structure of millerite phase of NiS using x-ray photoemission (XP) and Ultra-Violet photoemission (UP) measurements in conjunction with *ab inito* band structure as well as parameterized many-body calculations. The present results provide a consistent and quantitative description of the electronic structure

of the system. By comparing the hexagonal and millerite phases of NiS, we study the evolution of the spectral function with changing correlation effects in the metallic regime.

II. EXPERIMENTAL

For the preparation of the millerite samples, polycrystalline samples of hexagonal NiS was prepared first by solid state reaction [1,7]. Hexagonal NiS sample was then sealed in quartz tube in high vacuum and was maintained at 573 K for about 2-3 weeks and was cooled slowly to room temperature over a period of 8 hours, to obtain the millerite phase. The x-ray powder diffraction measurements confirmed the phase purity of the sample. Spectroscopic measurements were carried out in a combined VSW spectrometer with a base pressure of 2×10^{-10} mbar equipped with a monochromatized Al Kα x-ray source and a Helium discharge lamp. XP spectroscopic measurements were performed on the samples with an overall instrumental resolution of better than 0.8 eV, while UP measurements for He I and He II are performed with an instrumental resolution better than 90 meV and 120 meV, respectively. The sample surface was cleaned *in situ* periodically during the experiment by scraping with an alumina file and the surface cleanliness was monitored by recording the carbon 1s and oxygen 1s XP signal regions. The binding energy was calibrated to the instrumental Fermi-level which was determined by recording the Fermi-edge region from a clean silver sample.

III. CALCULATIONS

Scalar relativistic linearized muffin-tin orbital (LMTO) band structure calculations have been performed within the atomic sphere approximation (ASA) for millerite phase of NiS with the real crystal structure [5]. Here, the rhombohedral unit cell consisting of 3 formula units was employed. Sphere radii used for Ni and S were 2.49 and 2.55 a.u., respectively. 17 empty spheres with sphere radii in the range of 0.9 to 1.65 a.u. were also used. Convergence

was obtained with s, p and d orbitals at Ni and S atomic spheres and s and p for the empty spheres, with 220 k points in the irreducible part of the Brillouin zone.

Core level and valence band (VB) spectra were calculated for millerite NiS, using a NiS_5 cluster as found in the solid (see Fig. 1(b)), within a parameterized many-body model including orbital dependent electron-electron (multiplet) interactions. The calculational method has been described in detail elsewhere [8,9]. The calculations were performed including all the transition metal $3d$ and sulphur $3p$ orbitals. In the VB calculation, Ni $3d$ and S $3p$ contributions to the valence band spectra were calculated within the *same* model and with the *same* parameter values. As the dimension of the Hamiltonian matrix is large, Lanczos method was used to evaluate the spectral function and the calculated one-electron removal spectra were appropriately broadened to simulate the experimental spectra. In the Ni $2p$ core level calculation, Doniach-Šunjić line shape function [10] was used for broadening the discrete energy spectrum of the cluster model, in order to represent the asymmetric line shape of core levels from these highly metallic compounds; similar asymmetric line shapes are also found in the other core levels in this system. In the case of VB calculations, energy dependent Lorentzian function was used for the lifetime broadening. Other broadening effects such as the resolution broadening and solid state effects were taken into account by convoluting the spectra with a Gaussian function. The broadening parameters were found to be consistent with values used for similar systems [8,9,11]. Since the atomic cross-sections for the Ni $3d$ and S $3p$ states are vastly different, it is necessary to calculate a weighted average of these two contributions to the valence band. The atomic cross-section ratio [12] between S $3p$ and Ni $3d$ states (≈ 0.17) is not appropriate in this context, since solid-state effects alter this ratio significantly [13]. It was found that S $3p$/Ni $3d$ cross-section ratio of approximately 5.5 times that obtained from the atomic calculations gives the best result for the valence band calculations.

IV. RESULTS & DISCUSSIONS

The total as well as partial Ni d and S p densities of states (DOS) obtained from the LMTO band structure calculation are shown in Fig. 2. The thick solid line represents the total DOS, while thin solid line and dashed line show the Ni $3d$ and S $3p$ partial DOS, respectively. Our results are in good agreement with that of a previously published calculation [6]. The overall features of the DOS for millerite phase is similar to that obtained for the paramagnetic hexagonal phase of NiS [8]. However, in this case, the Fermi-level lies in the rising part of the DOS, instead of close to a minimum in DOS as in the case of hexagonal NiS where an instability in the Fermi-surface can open up a gap in certain directions of the Fermi-surface [1]. This distinction may partially be responsible for the absence of any phase transition in the millerite phase. The DOS between -3.5 eV and 1.2 eV is dominated by the Ni $3d$ contributions. Near the Fermi energy region, there is a substantial contribution from the S $3p$ states, due to the strong covalency (Ni d-S p interactions) in the system, forming the antibonding states. The DOS in the energy range -5.5 eV to -3.5 eV has dominant Ni $3d$ and S $3p$ contributions and represents the bonding states of the system. In the energy range, -8 eV to -5.5 eV, S $3p$ contribution is dominant with a smaller contribution from the Ni $3d$ states; these non-bonding states of the S $3p$ are stabilized in energy compared to Ni d-S p bonding states due to strong S-S interactions, similar to the case of hexagonal NiS and other sulphides [6]. The peak at ~ -1.9 eV resulting from the Ni $3d$ (t_{2g}-like states) is shifted to a higher energy compared to the t_{2g} states of the hexagonal NiS. This is related to the formation of the direct Ni-Ni bonds in the millerite phase leading to the stabilization of this phase compared to the hexagonal phase [6].

The band structure results are compared with the experimental data in Fig. 3. The partial densities of states of Ni $3d$ and S $3p$ are broadened with the experimental XP spectroscopic resolution of 0.8 eV and are shown along with valence band spectra taken with 21.2 eV (He I), 40.8 eV (He II) and 1486.6 eV (Al Kα) photon energies. Such a comparison provides an experimental determination of the orbital characters of the various features in

the experimental spectra, since the photoemission cross sections for Ni $3d$ and S $3p$ vary significantly with the photon energy. The decrease in the intensity of features B and C in going from 21.2 eV photon energy to 40.8 eV is explained by the Cooper minimum in the S $3p$ photoionization cross section at around 50 eV, indicating the dominance of the S $3p$ contributions in these two spectral features, with feature A dominated by the Ni $3d$ contribution. From band structure results, the feature B has contributions from S $3p$ as well as from Ni $3d$, while the feature C is dominated by S $3p$ states. Although the band structure calculations reproduce the features B and C rather well, the energy position of the feature A is not correctly reproduced, with the calculated peak appearing at about 0.4 eV higher binding energy compared to the experiment. This discrepancy between the experimental results and band structure calculations is attributed to the electron correlation effects within the Ni $3d$ levels; thus, it appears that correlation effects continue to have important influence even for this highly metallic system. This has prompted us to go beyond the band structure theories and study the electronic structure of this system using a cluster-model, where the electron correlation effects are explicitly taken into account.

The Ni $2p$ core level spectrum for the millerite phase of NiS is shown in the inset of Fig. 4 by solid circles. The spectrum consists of spin-orbit split $2p_{3/2}$ (852.8 eV binding energy) and $2p_{1/2}$ (870.2 eV binding energy) signals with strong satellite features at about 859.5 eV and 876 eV binding energies, corresponding to $2p_{3/2}$ and $2p_{1/2}$ signals, respectively. The intense satellite features in the Ni $2p$ core level spectrum point to the presence of the electron correlations in the system. The $2p_{3/2}$ and $2p_{1/2}$ peaks show strong asymmetries, similar to hexagonal form of NiS [8]. In order to determine the inelastic scattering background, we have performed electron energy loss spectroscopy (EELS) on these samples, with the same primary energy as that of the Ni $2p$ core level peak. Using a procedure that have been previously employed [8,9], the inelastic background function obtained for millerite NiS is shown in the inset of Fig. 4 as a solid line. The background function is a highly structured function with a broad plasmon loss feature around 876 eV, giving rise to an apparently stronger satellite intensity for the Ni $2p_{1/2}$ peak compared to the satellite intensity accompanying the $2p_{3/2}$

signal.

We have performed core and valence band calculations within a single model for a NiS_5 cluster. The cluster fragment used for the calculation is shown in Fig. 1(b). Within this model, we consider only one Ni atom; effects due to the strong Ni-Ni interactions present in this compound could not be considered due to the prohibitively large basis set involved in such calculations. For Ni^{2+}, the electron-electron interaction parameters, F^2_{dd}, F^4_{dd}, F^2_{pd}, G^1_{pd} and G^3_{pd} used were same as that for hexagonal form of NiS [8]. In the main panel of Fig. 4, we show the calculated core level spectrum (solid line) including the experimentally determined inelastic scattering background, superimposed on the experimental spectrum (open circles) for the parameter set S-Ni $(pd\sigma)$ = -1.8 eV, Δ = 1.0 eV and U_{dd} = 4.0 eV. The calculated spectrum without any broadening effect is presented as a stick diagram at the bottom of the same figure. The calculated spectrum matches reasonably well with the experimental spectrum. However, there are some differences between the calculated spectrum and the experimental one; the rising edge of the Ni $2p_{3/2}$ at $\sim$ 852 eV and the satellite energy region of the $2p_{1/2}$ peak are not accurately described by the calculation. Such discrepancies between the experimental and calculated spectrum may have its origin in the neglect of the strong metal-metal bonds in the system or due to the slight differences in the background function generated from the EELS spectrum and the actual background in the photoemission spectrum.

The $(pd\sigma)$ values obtained for millerite NiS (-1.8 eV) is considerably larger than that obtained for other Ni-S systems like, hexagonal NiS [8] ($(pd\sigma) = -1.4$ eV), NiS_2 [14] ($(pd\sigma) = -1.5$ eV) and $BaNiS_2$ [9] ($(pd\sigma) = -1.5$ eV). This significant increase in the $(pd\sigma)$ for the millerite case is related to the shorter Ni-S bonds in the system compared to the other nickel sulphides, as mentioned earlier, leading to a high degree of covalency. The value of the charge transfer energy (Δ = 1 eV) obtained for the millerite NiS is smaller than the hexagonal form of NiS [8] (2.5 eV) and NiS_2 [14] (2.0 eV). However, a similar value of Δ has been observed in another Ni-S system, $BaNiS_2$ [9] (Δ = 1.0 eV); significantly, $BaNiS_2$ has the same local geometry around Ni atoms as that in the millerite NiS with NiS_5 cluster in a

pyramidal arrangement. It has been observed in the case of divalent nickel oxides [11] that as the dimensionality of the Ni-O connectivity decreases, the charge transfer energy decreases, *via* a change in the Madelung potential. Thus, the decrease in the Δ for millerite phase compared to hexagonal NiS is also possibly due to a change in the Madelung potential arising from the decreased local coordination of Ni atoms. The lower value of Δ for the millerite phase compared to the hexagonal phase leads to a higher degree hybridization mixing of Ni d and S p states in the system, leading to an enhanced covalency. It turns out that the on-site Coulomb interaction strength, U, is very similar between millerite, hexagonal NiS [8] and NiS_2 [14]. This shows that U is not very sensitive to the local co-ordination or to the metallic/insulating property within the series of nickel sulphides. According to the ZSA [15] phase diagram, these parameters (small Δ and large hopping strength) place the millerite phase deep inside the pd-metallic regime.

Our calculations suggest that the ground state wavefunction of the millerite phase consists of 52%, 42.6% and 5.4% of d^8, $d^9\underline{L}$ and $d^{10}\underline{L}^2$ configurations with a high-spin $S = 1$ state. The average d-occupancy (n_d) of the system is found to be 8.53, which is substantially larger than that obtained for hexagonal NiS ($n_d = 8.43$). This establishes a strongly covalent ground state of the millerite phase, compared to other sulphides studied. In order to understand the origin of various features in the experimental core level spectrum, we have analyzed the characters of some typical final states, marked 1-10 in the main panel of Fig. 4, in terms of contributions from various configurations (d^8, $d^9\underline{L}^1$ and $d^{10}\underline{L}^2$) (see Table I). These features can be grouped into four regions; the main peak region, 852-855 eV (labelled 1-3 in Fig. 4), the weak satellite region between 856 eV and 858 eV (labelled 4 and 5), intense satellite region between 858 eV and 861 eV (labelled 6-8) and the high energy satellites beyond 863 eV (labelled 9 and 10). The first, third and fourth group of features have essentially similar characteristics as those in the hexagonal phase, with dominant $d^9\underline{L}^1$, significant contributions from all configurations, and dominant d^8 configuration, respectively [8]. However, the second group of features, which is absent in the hexagonal phase of NiS, have almost 90% of the contributions coming from the well-screened $d^9\underline{L}^1$ configuration. Al-

most pure charge transfer nature of these states is possibly due to the shorter Ni-S distances and a lower value of Δ.

Within the same model, we have calculated the XP valence band spectrum of the millerite phase. The calculated spectrum (solid line) along with Ni $3d$ (dashed line) and S $3p$ (dot-dashed line) contributions for the millerite phase are shown superimposed on the experimental XP valence band spectrum (open circles) in Fig. 5. The inelastic scattering background is taken to have an integral energy dependence and is shown as a dotted line. The Ni $3d$ contributions to the VB spectrum without any broadening effects are shown as a stick diagram. The parameter set used for the VB calculation is very similar to that used for the core level calculation; however, it was found that a $(pd\sigma)$ of -1.6 eV instead of -1.8 eV provides a better agreement with the experimental result. The agreement between the experimental and calculated spectra is reasonably good over the entire energy range. The features A and B are reproduced rather well, however, the feature C as well as the region close to the Fermi energy (lower binding energy side of the feature A) could not be described very accurately. This is however, not very surprising. The feature C is dominated by states arising from S p-S p interactions, as shown by the band structure results (see Fig. 3). Since we do not take this interaction in to account, and also due to the intrinsic limitation of a cluster model to account for such band structure effects, the feature C is completely absent in the results of the cluster model. It is reasonable to expect the features close to the E_F to be influenced by substantial Ni-Ni nearest-neighbor interactions present in this compound, explaining the discrepancy between the experiment and the results based on the cluster model neglecting such metal-metal interactions.

The analysis of the ground state wave function shows that the ground state has 55.2%, 40.4% and 4.4% of d^8, $d^9\underline{L}^1$ and $d^{10}\underline{L}^2$ configurations, respectively yielding an average occupancy of 8.49, with a high-spin configuration. The analysis of the final state configurations for a selected set (marked 1-10 in Fig. 5) of final states have been carried out and the results are given in table II. The various features can be grouped into different categories, namely the main peak region at 1-3 eV binding energy (labelled 1-3, corresponding to feature A),

region B in the range of 4-7 eV (labelled 4-7) and weaker satellites beyond 7 eV (labelled 8-10 and corresponding to feature D). The first group of features has the dominant contribution coming from the well screened $d^8\underline{L}^1$ states with a non-negligible contribution from the poorly screened d^7 states and overscreened $d^9\underline{L}^2$ states. These contributions are found to be similar to those observed in the case of hexagonal NiS [8]. The second group of features are predominantly contributed by $d^8\underline{L}^1$ and $d^9\underline{L}^2$ states, while in the case of hexagonal phase it was dominated by d^7 states. The third group of features have a high degree of d^7 character along with contributions from $d^9\underline{L}^2$ character, suggesting correlation effects within the Ni d states. These high energy, weak intensity satellites manifest in the valence band spectrum as a weak tailing of the spectrum beyond about 7 eV (feature D in Fig. 5). It is to be noted here that the characters of these weak intensity features are nearly same as that of the features appearing between 6 and 8 eV binding energy in the VB spectrum of hexagonal NiS which have been attributed to the spectral signature of the lower Hubbard band, persisting in the *pd*-metallic regime. Hence, the lower Hubbard band features are shifted to higher binding energies as well as becoming weaker in intensity in going from hexagonal NiS to millerite NiS, primarily due to an enhanced hopping strength in the millerite phase driving the system deeper in to the metallic regime.

Although the presence of the Hubbard bands in the metallic regime has been predicted by the dynamical mean-field theoretical (DMFT) calculations, the evolution of these spectral features well inside the metallic regime has not been studied in detail as a function of various electronic interaction strengths. A recent DMFT calculation for the spectral functions of a charge-transfer insulator near the metal-insulator transition boundary [16] suggests that within the metallic regime, the spectral signatures of the Hubbard band moves towards the Fermi-level, collapsing with the coherent states, forming the metallic ground state of the system with decreasing Δ. On the other hand, our experimental results establish that well inside the *pd*-metallic regime, the Hubbard band is further stabilized, moving towards higher binding energy region with increasing metallicity driven by enhanced hopping interaction strength between Ni d and S p states. Further experimental and theoretical efforts are

needed in this direction to have a better understanding of the evolution of the electronic structure of these systems.

In conclusion, the millerite phase of NiS has been studied by means of electron spectroscopic techniques, band structure and model Hamiltonian calculations. The band structure calculations were found to be more successful in describing the experimental valence band spectrum in comparison to the case of hexagonal NiS, suggesting a reduced effect of electron correlation in the millerite phase. This is consistent with the highly conducting ground state of the millerite phase, in contrast to the antiferromagnetic and poorly conducting ground state of hexagonal NiS. However, calculations including the electron correlation effects are found to be necessary for the description of certain features in the experimental spectra, indicating importance of such interaction effects even for such a highly metallic system. Thus, it appears that both band structure effects and correlation effects need to be treated on an equal footing for a complete description of such systems. The various electronic parameter strengths obtained from these calculations indicate that the millerite phase of NiS is a highly covalent metal (*pd*-metal). From the comparative study between hexagonal and millerite phases of NiS, the evolution of the spectral functions in a *pd*-metal as a function of the covalency is discussed.

V. ACKNOWLEDGMENTS

The authors thank Professor C. N. R. Rao for continued support and the Department of Science and Technology, and the Board of Research in Nuclear Sciences, Government of India, for financial support. SRK thanks Dr. P. Mahadevan for helpful discussions. DDS thanks Dr. M. Methfessel, Dr. A. T. Paxton, and Dr. M. van Schiljgaarde for making the LMTO-ASA band structure program available. The authors also thank Professor S. Ramasesha and the Supercomputer Education and Research Center, Indian Institute of Science, for providing the computational facility.

REFERENCES

⋆ Also at Jawaharlal Nehru Center for Advanced Scientific Research, Bangalore, India. Electronic address: sarma@sscu.iisc.ernet.in

[1] D. D. Sarma, S. R. Krishnakumar, Nirmala Chandrasekharan, E. Weschke, C. Schüßler-Langeheine, L. Kilian, and G. Kaindl, Phys. Rev. Lett. **80**, 1284 (1998).

[2] M. Nakamura, A. Sekiyama, H. Namatame, H. Kino, A. Fujimori, A. Misu, H. Ikoma, M. Matoba, and S. Anzai, Phys. Rev. Lett. **73**, 2891 (1994).

[3] F. Hulliger, J. Phys. Chem. Solids **26**, 639 (1965).

[4] R. Benoit, J. Chim. Phys. **52**, 119 (1955).

[5] N. H. Kolkmeijer and Th. A. L. Moesvelt, Z. Kristallorg., Kristallgeom., Kristallphys., Kristallchem. **80**, 91 (1931); J. D. Grice and R. B. Ferguson, Canad. Miner. **12**, 248 (1974); V. Rajamani and C. T. Prewitt, Canad. Miner. **12**, 253 (1974).

[6] P. Raybaud, J. Hafner, G. Kresse, and H. Toulhoat, J. Phys.: Condens. Matter. **9**, 11107 (1997).

[7] S. Anzai, M. Matoba, M. Hatori, and H. Sakamoto, J. Phys. Soc. Jpn. **55**, 2531 (1986).

[8] S. R. Krishnakumar, N. Shanthi, Priya Mahadevan, and D. D. Sarma, Phys. Rev. B **61**, 16370 (2000); S. R. Krishnakumar, N. Shanthi, Priya Mahadevan, and D. D. Sarma, Phys. Rev. B **62**, 10570(E) (2000).

[9] S. R. Krishnakumar, T. Saha-Dasgupta, N. Shanthi, Priya Mahadevan, and D. D. Sarma, Phys. Rev. B **63**, 045111 (2001).

[10] S. Doniach and M. Šunjić, J. Phys. C **3**, 285 (1970).

[11] K. Maiti, P. Mahadevan, and D. D. Sarma, Phys. Rev. B **59**, 12457 (1999).

[12] J. J. Yeh and I. Lindau, At. Data Nucl. Data Tables **32**, 1 (1985).

[13] D. D. Sarma, N. Shanthi and Priya Mahadevan, Phys. Rev. B **54**, 1622 (1996).

[14] S. R. Krishnakumar and D. D. Sarma, Unpublished results.

[15] J. Zaanen, G. A. Sawazky, and J. W. Allen, Phys. Rev. Lett. **55**, 418 (1985); D. D. Sarma, H. R. Krishnamurthy, Seva Nimkar, P. P. Mitra, S. Ramasesha and T. V. Ramakrishnan, Pramana - J. Phys. **38**, L531 (1992); Seva Nimkar, D. D. Sarma, H. R. Krishnamurthy, and S. Ramasesha, Phys. Rev. B **48**, 7355 (1993).

[16] H. Watanabe and S. Doniach, Phys. Rev. B **57**, 3829 (1998).

FIGURES

FIG. 1. (a) Schematic representation of the crystal structure of the millerite NiS. Dark spheres represent Ni atoms and grey spheres represent S atoms. (b) The local structural environment of the Ni atom which is penta-coordinated with S atoms in the millerite NiS.

FIG. 2. The total density of states (thick solid line) as well as partial Ni $3d$ (thin line) and S $3p$ (dashed line) density of states obtained from the LMTO band structure calculations for the millerite phase of NiS. The zero of the energy scale refers to the Fermi energy.

FIG. 3. Experimental valence band spectra of millerite NiS using 21.2 eV (He I), 40.8 eV (He II) and 1486.6 eV (XPS) photon energies along with the LMTO band structure partial DOS for Ni $3d$ and S $3p$, broadened by the experimental XP resolution function. Various features in the spectra are shown by the vertical lines and are labeled as A, B and C (see text).

FIG. 4. The Ni $2p$ core level spectrum of the millerite NiS (solid circles) along with the generated inelastic scattering background function from the EELS spectrum at the same primary beam energy are shown in the inset. In the main panel, experimental Ni $2p$ spectrum (open circles) along with the calculated spectrum (solid line) for millerite NiS obtained from the cluster calculation are shown. Various final states of the cluster calculation and the corresponding intensity contributions without any broadening are shown as the stick diagrams.

FIG. 5. The experimental VB spectrum (open circles) along with the calculated spectrum (solid line), Ni $3d$ component (dashed line), S $3p$ component (dot-dashed line) and the integral background (dotted line) are shown for millerite NiS. The final states of the calculation and the corresponding intensities without any broadening are shown as the energy stick diagrams.

TABLES

TABLE I. Contributions from various configurations in the final states of the Ni $2p$ core level photoemission in millerite NiS. The peak numberings correspond to the labels indicated in Fig. 4; the corresponding binding energies (BE) in eV are also shown.

Peak no.	1	2	3	4	5	6	7	8	9	10
BE	852.9	853.7	854.3	857.2	857.4	859.0	859.7	860.7	864.8	866.4
d^8	16.48	12.57	10.06	4.77	6.35	26.67	28.96	22.91	60.43	72.18
$d^9\underline{L}^1$	57.35	58.53	56.63	90.58	87.05	44.58	29.89	33.25	30.84	23.81
$d^{10}\underline{L}^2$	26.17	28.90	33.41	4.65	6.60	28.75	41.15	43.84	8.73	4.01

TABLE II. Contributions from various configurations in the final states of valence band photoemission in millerite NiS. The peak numberings correspond to the labels indicated in Fig. 5; the corresponding binding energies (BE) in eV are also shown.

Peak no.	1	2	3	4	5	6	7	8	9	10
BE	1.4	1.67	2.18	4.40	4.83	5.12	6.23	7.64	8.33	8.57
d^7	16.70	14.64	9.34	0.94	1.69	0.90	4.3	39.66	32.55	26.98
$d^8\underline{L}^1$	53.93	53.70	52.81	66.49	64.14	71.58	59.25	10.12	13.39	17.56
$d^9\underline{L}^2$	26.90	28.96	34.36	31.99	33.37	26.98	35.68	41.44	38.94	41.08
$d^{10}\underline{L}^3$	2.47	2.70	3.49	0.58	0.80	0.54	0.77	8.78	15.12	14.38

(a)

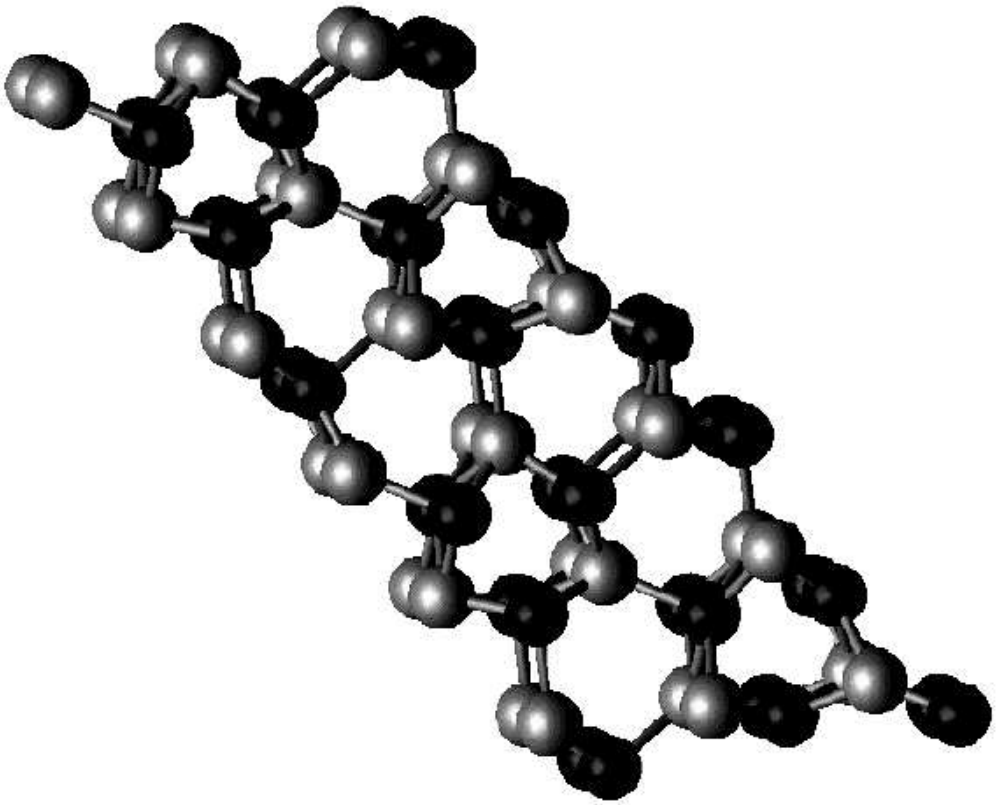

(b)

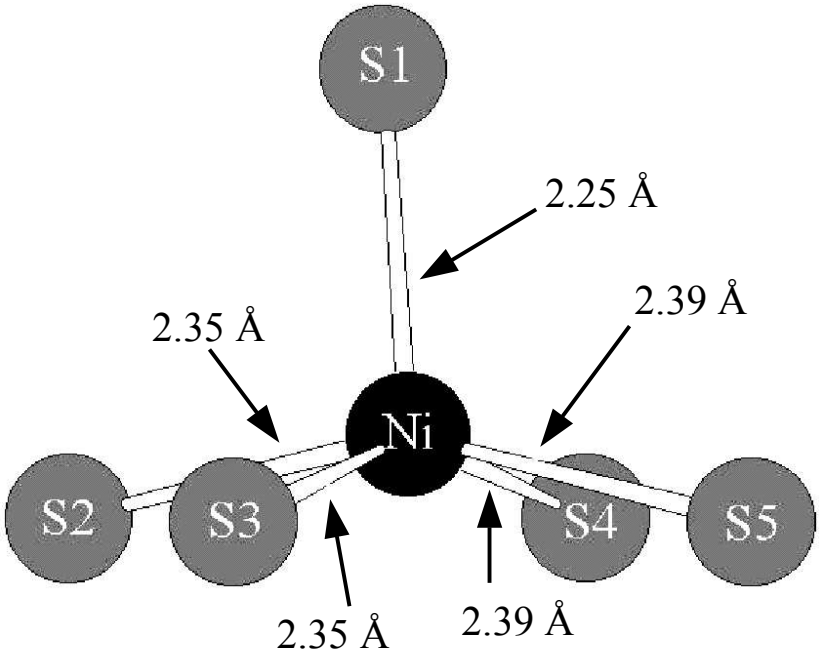

Krishnakumar *et al*., Fig. 1

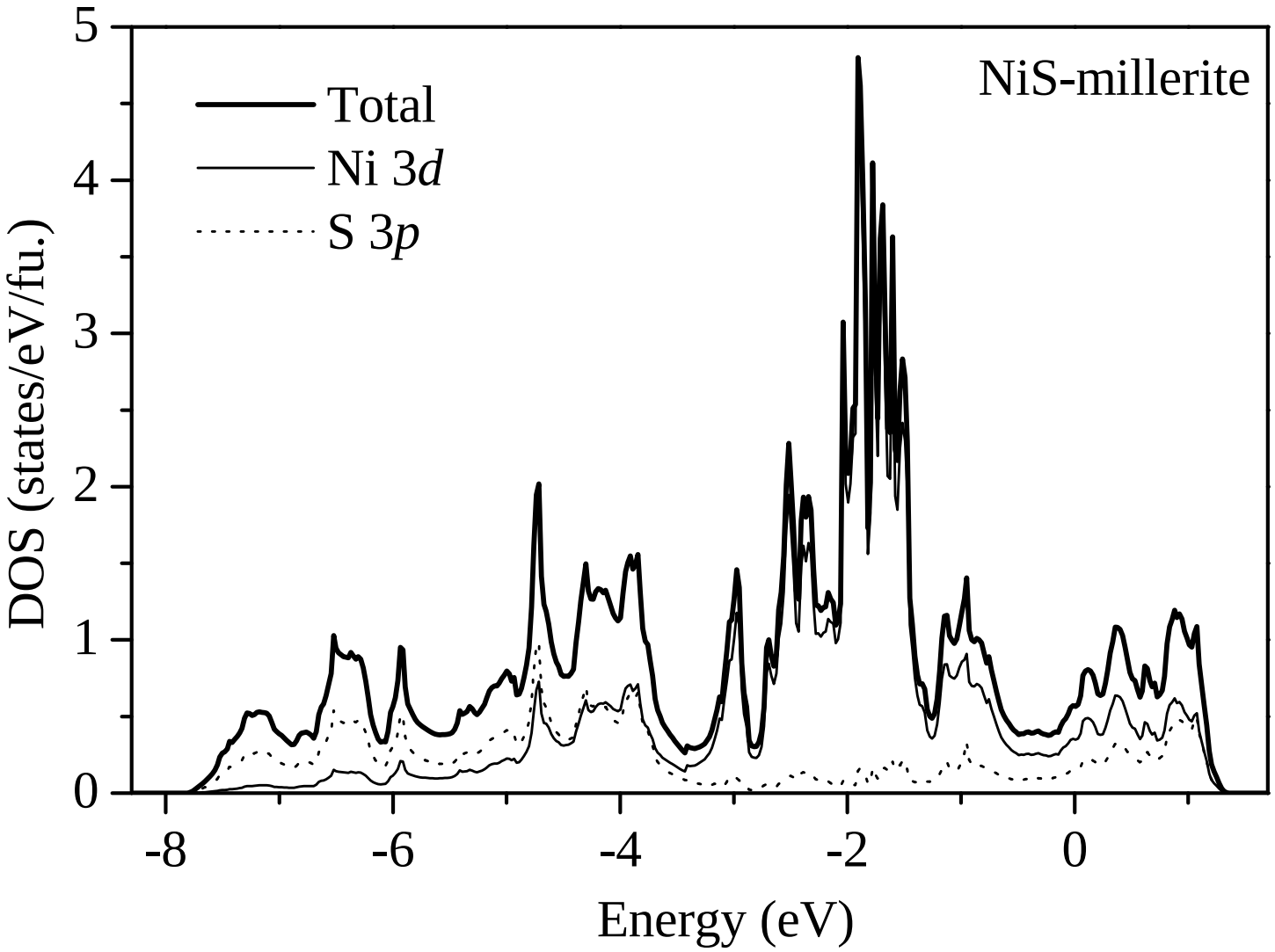

Krishnakumar *et al*., Fig. 2

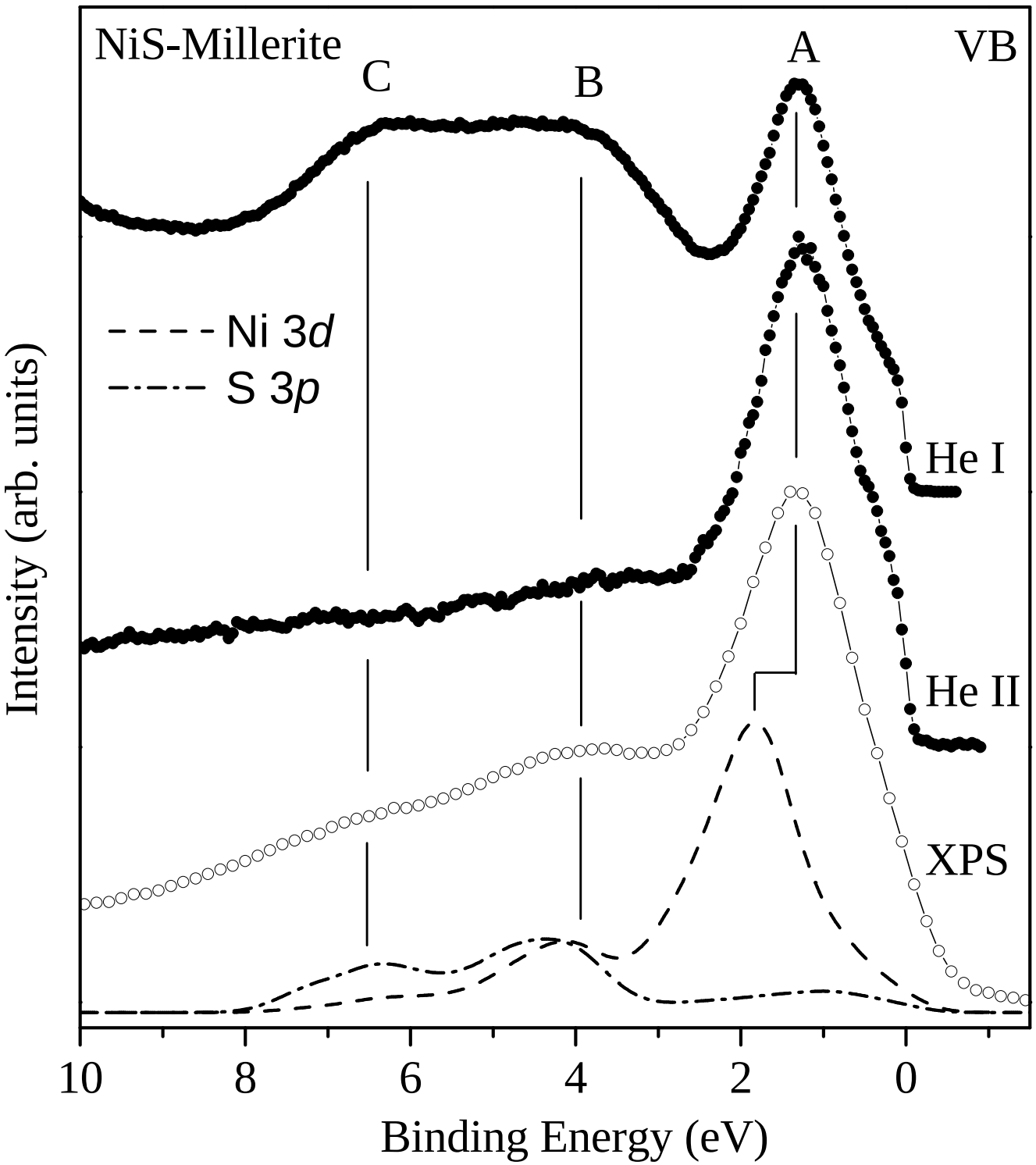

Krishnakumar *et al.*, Fig. 3

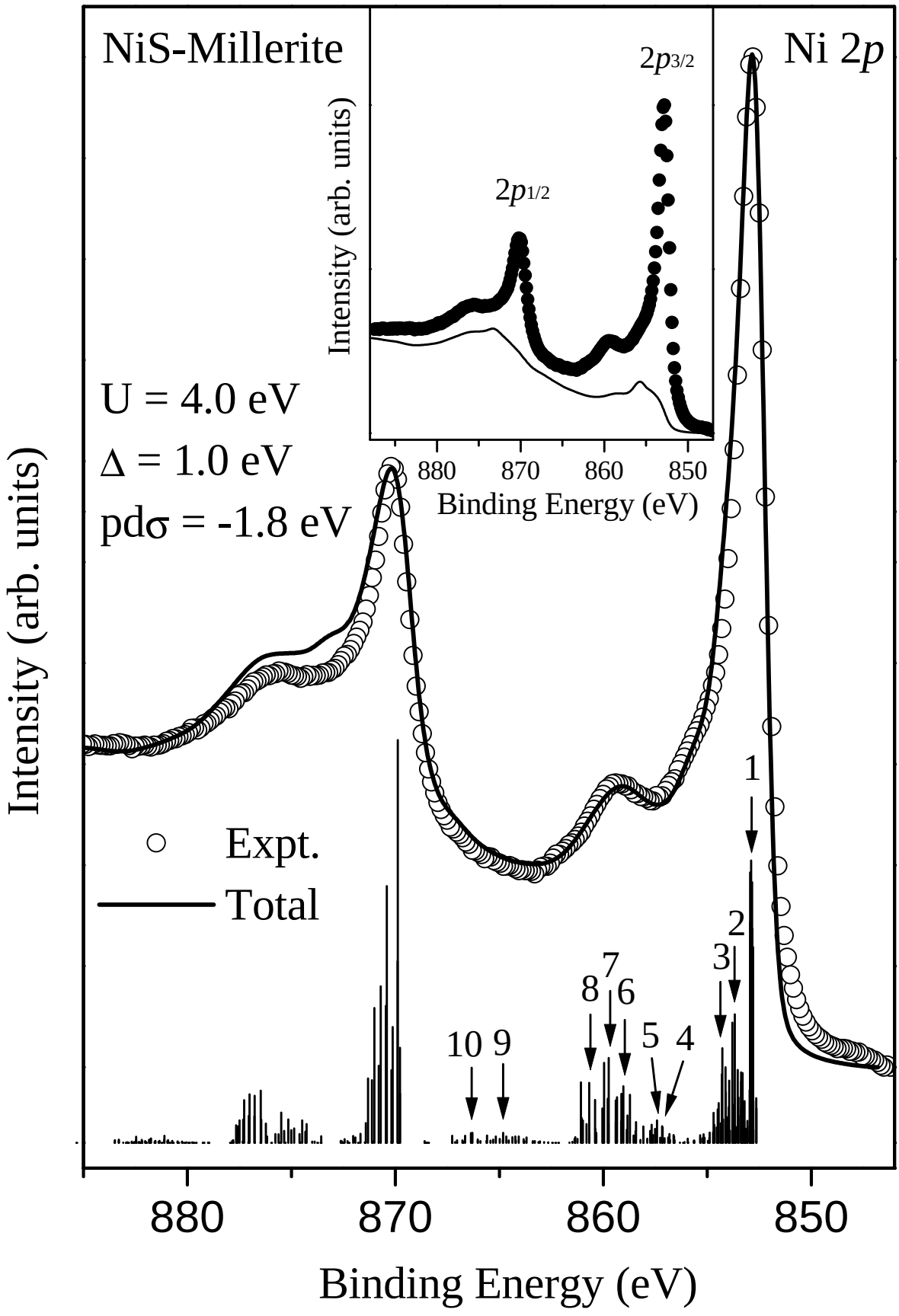

Krishnakumar *et al.*, Fig. 4

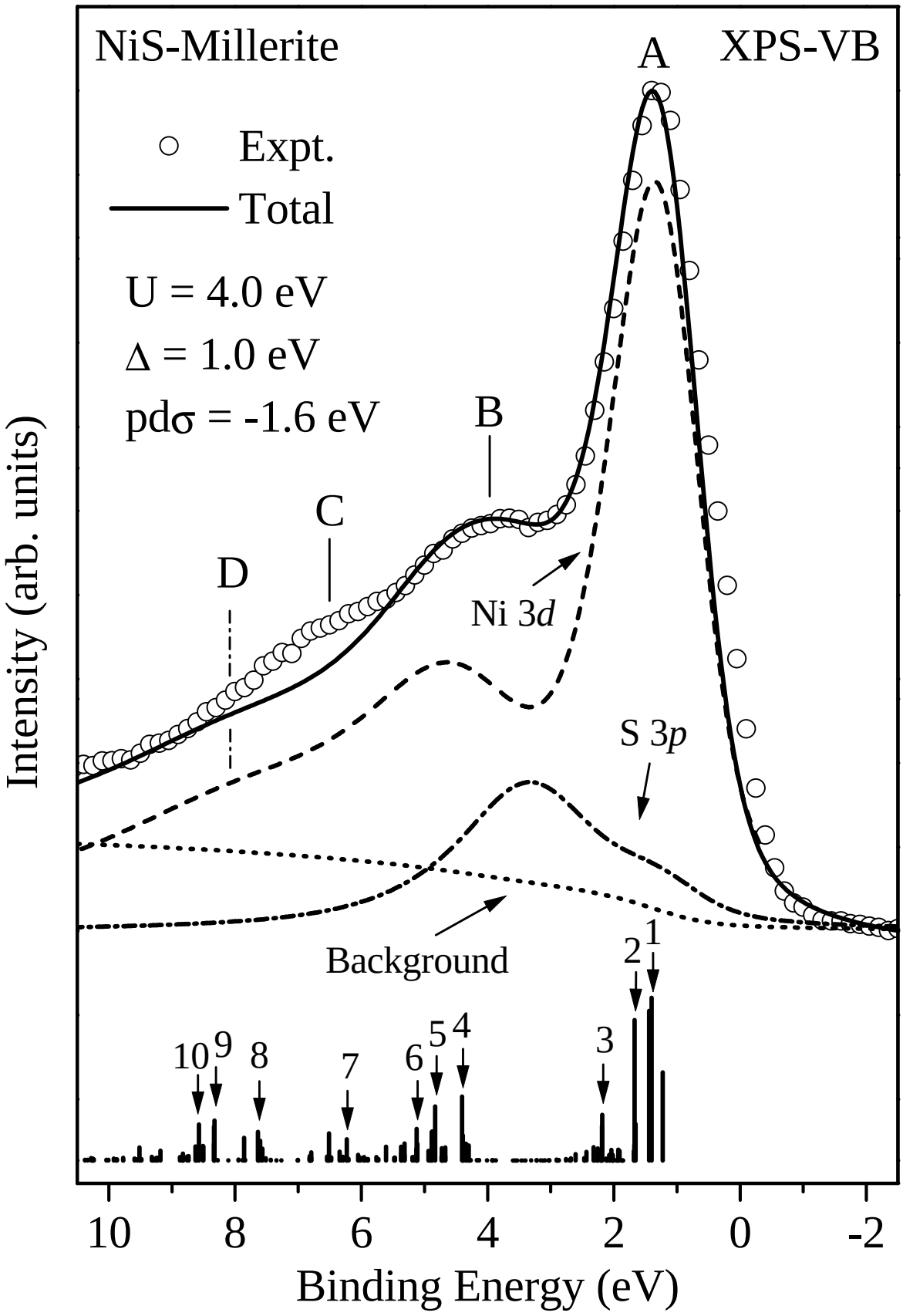

Krishnakumar *et al.*, Fig. 5